PREPRINT 483

OCTOBER 2018

igpm | RWTH AACHEN UNIVERSITY

Coupling of compressible Euler equations

Michael Herty, Siegfried Müller and Aleksey Sikstel

Institut für Geometrie und Praktische Mathematik
Templergraben 55, 52062 Aachen, Germany

Institut für Geometrie und Praktische Mathematik, RWTH Aachen University, Templergraben 55, D-52056 Aachen, Germany;
Email: herty@googlemail.com.de, mueller@igpm.rwth-aachen.de, sikstel@igpm.rwth-aachen.de

Coupling of compressible Euler equations

Michael Herty · Siegfried Müller · Aleksey Sikstel

Abstract The Riemann problem for coupled Euler equations is analysed. The coupling conditions at a steady interface impose continuous pressure and temperature while momentum differs. The outtake of the momentum models the influence of a gas-powered generator linked to a high-pressure gas network. We prove the existence and uniqueness of the solution to the coupled Riemann problem in case the drop in the momentum is sufficiently small. Furthermore, we analyse the coupling problem for the special case of isentropic Euler equations and obtain similar results. The behaviour of coupled isentropic and coupled compressible Euler equations is compared numerically.

Keywords Gas networks · compressible Euler equations · isentropic Euler equations · coupling conditions · coupled Riemann problem · Lax curves

1 Introduction

Coupled systems of one-dimensional hyperbolic balance laws have recently gained interest in the engineering and mathematical community due to numerous applications and we refer e.g. to [3] for a recent overview in this field. We are interested in the modeling and simulation of high–pressure gas pipeline systems, that have been studied e.g. in [30, 2, 4, 26]. The coupled system proposed in this work is in part inspired by questions arising in combined natural gas and electricity networks. The integration of both sectors has gained recent interest in the engineering community due to the rise of combined cycle natural gas thermal power plants [13, 36, 1, 40, 31]. For instance, a dramatic change on the gas pipelines in the north–east of the US has been observed where natural gas-fired electrical generation increased from 5% of total capacity to

This work has been supported in part by the German Research Council (DFG) within the DFG Collaborative Research Center SFB-TR-40, TP A1, DFG Cluster of Excellence 'Production technologies for high–wage countries' HE5386/13,14,15-1, DFG Research Training Group 'Energy, Entropy, and Dissipative Dynamics' DFG-GRK 2326, KI-Net NSF RNMS grant No. 1107444, DAAD–MIUR project, and Bundesministerium für Bildung und Forschung 05M18PAA.

M. Herty
E-mail: herty@igpm.rwth-aachen.de

S. Müller
E-mail: mueller@igpm.rwth-aachen.de

A. Sikstel
E-mail: sikstel@igpm.rwth-aachen.de

Institut für Geometrie und Praktische Mathematik
RWTH Aachen University
Templergraben 55, 52056 Aachen, Germany

50% in only two decades [40]. Similar changes are observed in Brazil, Europe and expected in other countries also due to the parallel development in electrical grids to expand intermittent renewable generation such as solar and wind power. Consequently, it is expected that electric power plants become one of the major natural gas consumers and the modeling of high–pressure gas pipelines need to account for those influences in order to meet the requirements for natural gas flows in pipelines. In general, the modeling of natural gas-fired power generator involves two networks: the natural gas transportation and the electric transmission network [36, 1, 40, 5]. We are interested in the effect of the gas-fired generator on the natural gas transportation network and we are in particular interested in the fine–scale resolution of the resulting flow pattern in the gas network. Therefore, we consider a fine–scale model given by the Euler equations for such a dynamics. The relevant regime and the underlying scaling leading to such a model can be found e.g. in [4]. Depending on the level of detail relevant to the operator simplified models as e.g. the p-system or algebraic–differential equations might be employed [21, 18, 39, 28, 33, 38].

The gas–fired generator is usually a turbine and there exist many detailed models to describe turbine action dynamics, see e.g. [25, 32, 27]. However, the impact of the gas turbine on the gas transmission network can be modelled by conditions that leave pressure and temperature of the transmitted gas constant and only account for the mass loss due to the turbine action [5]. Clearly, this mass loss induces pressure fluctuations along the gas network which we analyse using the Euler equations and the p-system, respectively. We focus here on the mathematical aspects and influence of the turbine on the adjacent transmission network. So far, in mathematical literature only compressors and valves have been considered [20, 23, 8, 34, 12, 39]. Compared to this analysis our contributions are different in two aspects: first, we consider the full Euler system and second, we do not have mass conservation across a gas–fired turbine. On the contrary it is reasonable to assume that strong time–dependent changes appear according to the demand of the electricity network. This leads to pressure fluctuations along the natural gas pipe network. Compared to the analysis of the coupled Euler system in [9] we do not assume mass conservation and we present explicit formulas to construct solutions usable in numerical schemes. Furthermore, we present numerical results that where absent in [9]. However, the analysis of the coupled system is driven by the recent advances in this direction and it relies as many of the presented approaches on detailed analysis of suitable Riemann problems. We refer again to [3] for a detailed review of the literature on this topic.

2 Coupled Riemann Problem for the Euler equations

We analyse the mathematical properties of coupled Euler equations. The coupling conditions imposed will be used as a fine-scale model for turbine effects on high-pressure gas networks as motivated in the previous section. The following part is devoted to the mathematical analysis and the solvability of the coupled problem. The derived formulas will also serve as a numerical method later on. The problem will be set up as follows: two one-dimensional, compressible gas flows are coupled at position $x = 0$ such that the momentum $\rho v(t, x = 0)$ has a negative jump of magnitude $\varepsilon \in \mathbb{R}^+$ while the pressure at the interface $p(t, x = 0)$ as well as the temperature $T(t, x = 0)$ are assumed to be continuous. As a convention it is assumed that the gas flows in positive direction, i.e. $\rho v \geq 0$. To distinguish the left state (inflow) from the right state (outflow) we denote the states with or without bar, respectively. Then the coupling conditions read

$$\begin{aligned} \overline{\rho v} &= \rho v + \varepsilon, \\ \overline{p} &= p, \\ \overline{T} &= T. \end{aligned} \tag{1}$$

Here, ε models the outtake of gas to the turbine. This mass flow is converted to electric power by the turbine. Usually, the gas turbines are external and therefore do not influence the pressure and the temperature of the gas inside the pipes. In applications as well as in our numerical results ε will be time dependent. This does not restrict the following discussion. The gas flow is modelled

by the compressible Euler equations in one spatial dimension

$$\frac{\partial \rho}{\partial t} + \frac{\partial \rho v}{\partial x} = 0, \tag{2}$$

$$\frac{\partial \rho v}{\partial t} + \frac{\partial}{\partial x}(\rho v^2 + p) = 0, \tag{3}$$

$$\frac{\partial \rho E}{\partial t} + \frac{\partial}{\partial x}\left(\rho v (E + p/\rho)\right) = 0, \tag{4}$$

where $E = \rho e + \frac{1}{2}\rho v^2$ denotes the total energy per unit volume and e the internal energy per unit mass. The system is closed by the ideal gas law

$$p = \rho R T = \rho e(\gamma - 1) \tag{5}$$

with specific gas constant R and the constant ratio of specific heat capacities $\gamma \geq 1$. Thus the speed of sound is given by

$$c = \sqrt{\frac{\gamma p}{\rho}}. \tag{6}$$

Furthermore, the flow at the coupling interface is assumed to be *subsonic*, that is $|v(t, x = 0^{\pm})| < c(t, x = 0^{\pm})$. This assumption is typically satisfied in high-pressure gas networks, see [2,30]. The construction of a solution by means of a Riemann problem (RP) is described in following and the formulas are given in the Appendix. A RP is a Cauchy problem where the initial data is constant except for a single discontinuity that, without loss of generality, is located at $x = 0$. The solution of the RP for compressible Euler equations is well-known and can be found in classical textbooks, e.g. in [35,16,10]. The main idea is to connect the two constant initial states via three Lax curves in the phase space that correspond to the three characteristic k-fields, $k = 1, 2, 3$. This results in a nonlinear system of three equations. The 1-wave and the 3-wave corresponding to the 1-field and the 3-field, respectively, are composed of two branches related to a rarefaction wave (RW) or a shock wave (SW). However, the 2-wave is a contact discontinuity across which the pressure p and the velocity v remain constant while other physical quantities may exhibit a discontinuity. This fact is exploited to transform the system of three equations into a scalar equation by projecting the three-dimensional phase space to the pressure-velocity space. More precisely the compressible Euler equations are transformed to primitive variables $\boldsymbol{u} := (\rho, v, p)^T$ and the Lax curves are parameterised by the pressure p. The resulting scalar equation consists of the difference of the velocity curves corresponding to the forward 1-wave and the backward 3-wave Lax curve. The unique solution of the resulting scalar equation is the pressure that determines the intermediate states. The Lax curves in primitive variables are listed in equations (49), (50) and (61), (62) in the Appendix A.

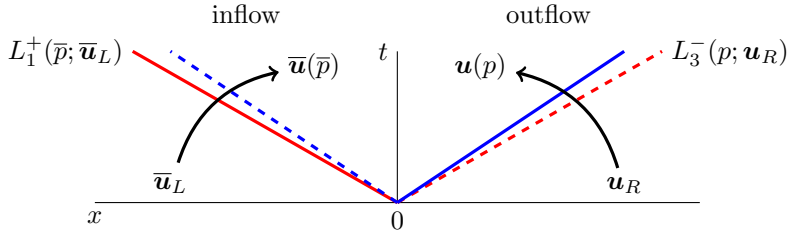

Fig. 1 Wave structure in the t-x-plane. $\overline{\boldsymbol{u}}_L$ and $\boldsymbol{u}_R$ - constant initial states at the in- and outflow, respectively. L_1^+ - 1-wave forward Lax curve, L_3^- - 3-wave backward Lax curve. $\overline{\boldsymbol{u}}(\overline{p})$ and $\boldsymbol{u}(p)$ - states connected via the Lax curve to the initial data $\overline{\boldsymbol{u}}_L$ and $\boldsymbol{u}_R$, respectively.

We employ a similar construction to obtain a solution to the coupling problem. Given the subsonic states $\overline{\boldsymbol{u}}_L$ at the inflow and $\boldsymbol{u}_R$ at the outflow the solution of the coupling problem is

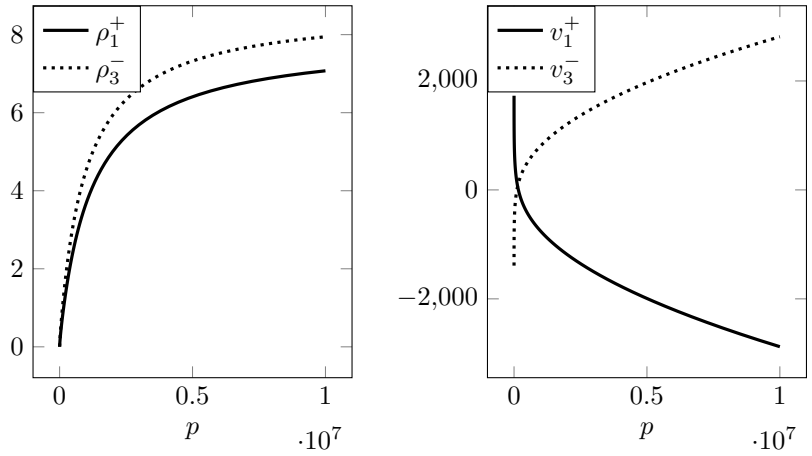

Fig. 2 Left: densities along the 1- and 3-wave in positive and negative direction, respectively. Right: Intersection of wave curves in the v-p plane.

defined as the solution of two half–RPs $\overline{\boldsymbol{u}}(\bar{p})$ and $\boldsymbol{u}(p)$ that satisfy the coupling conditions (1), see [22].

We recall some basic properties of conservation laws of the type

$$\partial_t \boldsymbol{w} + \partial_x f(\boldsymbol{w}) = 0,\ x \in \mathbb{R},\ t \geq 0 \tag{7}$$

for $\boldsymbol{w} \in \mathbb{R}^m$. For initial data $\boldsymbol{w}(0,x)$ given by two constant states $\overline{\boldsymbol{u}}_L$ for $x < 0$ and $\boldsymbol{u}_R$ for $x > 0$, sufficiently close, the problem admits an entropy weak solution composed of $m+1$ constant states separated by m elementary waves [10]. The solution can therefore be written as $\boldsymbol{w} = \boldsymbol{w}(\frac{x}{t}; \overline{\boldsymbol{u}}_L, \boldsymbol{u}_R)$. We assume equation (7) holds for $x > 0$ and initial data $\boldsymbol{w}(x,0) = \boldsymbol{u}_R$ for $x > 0$. Also, we assume equation

$$\partial_t \bar{\boldsymbol{w}} + \partial_x \bar{f}(\bar{\boldsymbol{w}}) = 0, \tag{8}$$

holds for $\bar{\boldsymbol{w}} \in \mathbb{R}^{\bar{m}}$, a possibly different flux function $\bar{f}$ and initial data $\boldsymbol{w}(x,0) = \overline{\boldsymbol{u}}_L$ for $x < 0$. At the point $x = 0$ we prescribe a general condition $\Psi = 0$ where $\Psi : \mathbb{R}^{\bar{m}+m} \to \mathbb{R}^{\ell}$. As weak solution to the coupled problem we understand a pair of weak entropy solutions $\bar{\boldsymbol{w}}(x,t), \boldsymbol{w}(x,t)$ to equation (8) and equation (7) for $x < 0$ and $x > 0$, respectively. Further the trace at $x = 0$ fulfills a.e. in t the coupling condition, i.e.,

$$\Psi(\bar{\boldsymbol{w}}(0-,t), \boldsymbol{w}(0+,t)) = 0,\ t > 0. \tag{9}$$

We refer to [8] for a precise definition in the case of 2×2 conservation laws. Note that in the case $\ell = \bar{m} = m$, $f = \bar{f}$ and $\Psi(\bar{\boldsymbol{w}}, \boldsymbol{w}) = \bar{f}(\bar{\boldsymbol{w}}) - f(\boldsymbol{w})$ the solution should coincide with the solution to a classical RP for the initial data $\overline{\boldsymbol{u}}_L$ and $\boldsymbol{u}_R$.

A half–RP associated with equation (8) on $(-\infty, 0)$ consists of the solution $\overline{\boldsymbol{w}}$ to the RP for equation (8) with initial data $\overline{\boldsymbol{w}}(x,0) = \overline{\boldsymbol{u}}_L$ for $x < 0$, and $\overline{\boldsymbol{w}}(x,0) = \overline{\boldsymbol{v}}$ for $x > 0$ *restricted to* $x < 0$. Similarly, we can consider a half–RP associated with equation (7) on $(0, \infty)$ with initial data $\boldsymbol{w}(x,0) = \boldsymbol{v}$ for $x < 0$ and $\boldsymbol{w}(x,0) = \boldsymbol{u}_R$ for $x > 0$ by *restriction* to $x > 0$. Particularly interesting solutions in view of the coupling conditions are solutions to the half–RP where on $(-\infty, 0)$ the trace of the solution fulfills $\overline{\boldsymbol{w}}(0-,t) = \overline{\boldsymbol{v}}$ and on $(0, \infty)$ the trace of the solution fulfills $\boldsymbol{w}(0+,t) = \boldsymbol{v}$.

In the following we will only consider those solutions. They exist provided that $\overline{\boldsymbol{v}}$ and $\boldsymbol{v}$ are suitably chosen. Given a state $\overline{\boldsymbol{u}}_L$ we introduce the notion of admissible boundary states $\overline{\boldsymbol{v}}$ as follows. For a given constant state $\overline{\boldsymbol{u}}_L$ the set of admissible boundary data $\bar{V}(\overline{\boldsymbol{u}}_L)$ consists of states $\overline{\boldsymbol{v}} \in \bar{V}(\overline{\boldsymbol{u}}_L)$ such that the solution to the half–RP on $(-\infty, 0)$ fulfills $\overline{\boldsymbol{w}}(0-,t) = \overline{\boldsymbol{v}}$. Similarly, for a given state $\boldsymbol{u}_R$ the set of admissible boundary data $V(\boldsymbol{u}_R)$ consists of states $\boldsymbol{v} \in V(\boldsymbol{u}_R)$ such that the solution to the half–RP on $(0, \infty)$ fulfills $\boldsymbol{w}(0+,t) = \boldsymbol{v}$.

Definition 1 Having the sets $\bar{V}(\overline{\boldsymbol{u}}_L)$ and $V(\boldsymbol{u}_R)$ at hand the solution to the coupled problem is constructed as follows: we need to prove that there exist unique states $\overline{\boldsymbol{v}} \in \bar{V}(\overline{\boldsymbol{u}}_L)$ and $\boldsymbol{v} \in V(\boldsymbol{u}_R)$ such that $\Psi(\overline{\boldsymbol{v}}, \boldsymbol{v}) = 0$. Provided we have such states the **solution to the coupled problem** is given by the solution to the two half–RPs with the corresponding initial data $(\overline{\boldsymbol{u}}_L, \overline{\boldsymbol{v}})$ and $(\boldsymbol{v}, \boldsymbol{u}_R)$, respectively.

Due to the definition of the sets $V(\boldsymbol{u}_R), \bar{V}(\overline{\boldsymbol{u}}_L)$, the trace of the solution fulfills the coupling condition. In order to obtain the solution to the half–RPs we consider states on the p-parameterised Lax curves corresponding to the forward $(^+)$ and the backward $(^-)$ i-wave: $L_i^{\pm}(p; \boldsymbol{u}) := (\rho_i^{\pm}, v_i^{\pm}, p)^T$ originating from $\tilde{\boldsymbol{u}} := (\tilde{\rho}, \tilde{v}, \tilde{p})^T$, i.e. $L_i^{\pm}(\tilde{p}; \tilde{\boldsymbol{u}}) = \tilde{\boldsymbol{u}}$, $i = 1, 2, 3$. Since the 2-wave is a contact discontinuity, the admissible interfacial states $\overline{\boldsymbol{u}}(p)$ and $\boldsymbol{u}(p)$ lie on $L_1^-(\cdot; \overline{\boldsymbol{u}}_L)$ and $L_3^+(\cdot; \boldsymbol{u}_R)$. This guarantees that the solution to the half–RP has solutions propagating to $x > 0$ and $x < 0$, respectively [11, 15].

Applying the ideal gas law (5) the coupling conditions (1) can be rewritten as

$$\begin{aligned} \overline{p} &= p, \\ \overline{\rho} &= \rho, \\ \overline{v} &= v + \frac{\varepsilon}{\overline{\rho}}. \end{aligned} \tag{10}$$

Note that the continuity of mass is implied by (1) and (5). Thus, the coupling condition on the momentum is replaced by a condition on the velocity v. Plugging in the states at the corresponding Lax curves into (10) the coupling conditions read

$$\begin{aligned} \rho_1^+(\overline{p}; \overline{\boldsymbol{u}}_L) &= \rho_3^-(p; \boldsymbol{u_R}), \\ v_1^+(\overline{p}; \overline{\boldsymbol{u}}_L) &= v_3^-(p; \boldsymbol{u_R}) + \frac{\varepsilon}{\rho_1^+(\overline{p}; \overline{\boldsymbol{u}}_L)}. \end{aligned} \tag{11}$$

Since the density on the Lax curve $\rho_i^{\pm}$ is independent of $v_i^{\pm}$ the coupling condition corresponding to the continuity of the density is satisfied for any p and the coupling conditions are reduced to one equation. Incorporating (11) we finally obtain a single equation for one unknown. For this purpose we define the function

$$g_\varepsilon \colon \mathbb{R} \to \mathbb{R}, \quad p \mapsto \underbrace{v_1^+(\overline{p}; \overline{\boldsymbol{u}}_L) - v_3^-(p; \boldsymbol{u}_R)}_{=: g_\varepsilon^1(p)} - \underbrace{\varepsilon \tau_1^+(p; \overline{\boldsymbol{u}}_L)}_{=: g_\varepsilon^2(p)} \tag{12}$$

for fixed states $\overline{\boldsymbol{u}}_L$ and $\boldsymbol{u}_R$. Here $\tau_i^{\pm} := 1/\rho_i^{\pm}$ denotes the specific volume. Then solving the coupling problem (11) is equivalent to solving the scalar nonlinear equation

$$g_\varepsilon(p) = g_\varepsilon^1(p) - g_\varepsilon^2(p) = 0. \tag{13}$$

In case of $\varepsilon = 0$, the coupling problem corresponds to the classical RP that has a unique solution if vacuum is admitted. Note that in the present work we only consider initial states that do not result in a vacuum solution for the RP.

Proposition 1 (Solution of the classical RP) *Assume that*

$$v_L + \frac{2c_L}{\gamma - 1} > v_R - \frac{2c_R}{\gamma - 1} \tag{14}$$

holds then the classical RP has a unique solution that is not vacuum.

Proof In the setting of the classical RP the function g_ε reduces to

$$g_0(p) = g_0^1(p) = v_1^+(p; \boldsymbol{u}_L) - v_3^-(p; \boldsymbol{u}_R). \tag{15}$$

The limits of $v_i^{\pm}$ listed in Table 1 in the Appendix A imply the following properties of the velocity:

1. v_1^+ is strictly decreasing and convex:

$$v_1^+(0; \boldsymbol{u}_L) = v_L + \frac{2c_L}{\gamma - 1} > -\infty = \lim_{p \to \infty} v_1^+(p; \boldsymbol{u}_L). \tag{16}$$

2. $(v_1^+)'$, the first derivative of v_1^+ with respect to p, is negative:

$$(v_1^+)'(0;\boldsymbol{u}_L) = -\infty < 0^- = \lim_{p\to\infty}(v_1^+)'(p;\boldsymbol{u}_L). \tag{17}$$

3. v_3^- is strictly increasing and concave:

$$v_3^-(0;\boldsymbol{u}_R) = v_R - \frac{2c_R}{\gamma-1} < \infty = \lim_{p\to\infty} v_3^-(p;\boldsymbol{u}_R). \tag{18}$$

4. $(v_3^-)'$, the first derivative of v_3^- with respect to p, is positive:

$$(v_3^-)'(0;\boldsymbol{u}_R) = \infty > 0^+ = \lim_{p\to\infty}(v_3^-)'(p;\boldsymbol{u}_R). \tag{19}$$

Note that $v_i^\pm$ corresponds to a rarefaction wave solution and a shock wave solution in case p tends to 0 and to ∞, respectively. Because we have assumed that no vacuum states are admitted and since v_1^+ is strictly decreasing and v_3^- is strictly increasing there exists a unique root of g_0, see Figure 2.

□

Since there exists a unique solution of $g_\varepsilon(p) = 0$ for $\varepsilon = 0$ we may obtain locally the existence of a solution for $\varepsilon > 0$.

Theorem 1 (Local solutions of $g_\varepsilon(p) = 0$) *Let $\varepsilon \geq 0$ be sufficiently small. Then, in a neighbourhood of the solution to the classical RP, there exists a unique root of g_ε solving the coupling conditions* (1).

Proof To prove the local existence of a solution of (13) for $\varepsilon > 0$ we make use of the implicit function theorem. For this purpose note that $g_\varepsilon \in C^2(\mathbb{R}^2,\mathbb{R})$ as a mapping

$$g\colon \mathbb{R}^+ \times \mathbb{R}_0^+ \to \mathbb{R}, (p,\varepsilon) \mapsto g(p,\varepsilon;\overline{\boldsymbol{u}}_L,\boldsymbol{u}_R) \equiv g_\varepsilon(p). \tag{20}$$

Let p_0 denote the unique root of g_ε in case of $\varepsilon = 0$, i.e. $g_0(p_0) = 0$ according to Proposition 1. Since by (17) and (19)

$$\frac{\partial g}{\partial p}(p_0,0;\overline{\boldsymbol{u}}_L,\boldsymbol{u}_R) = \left(v_1^+(p_0;\overline{\boldsymbol{u}}_L)\right)' - \left(v_3^-(p_0;\boldsymbol{u}_R)\right)' < 0 \tag{21}$$

there exist open neighbourhoods $U(p_0) \subset \mathbb{R}$, $V(0) \subset \mathbb{R}$ and a continuously differentiable map $p : V(0) \to U(p_0)$ such that for all $\varepsilon \in V(0)$

$$g(p(\varepsilon),\varepsilon;\overline{\boldsymbol{u}}_L,\boldsymbol{u}_R) = 0. \tag{22}$$

□

Definition 2 Theorem 1 implies that in the neighbourhood of $(p_0, 0)$ there exists a family of unique one-parametric solutions of $g_\varepsilon(p) = 0$. Since $p(\varepsilon) \in C^1(V(0), U(p_0))$, i.e. these solutions depend continuously on the *unique* solutions of the classical RP, we will call them **physically admissible**.

Theorem 1 guarantees the existence of a local solution to $g_\varepsilon(p) = 0$, in a neighbourhood of the solution of the classical RP. In the next theorem we show that for $\varepsilon > 0$ in fact g_ε can have two roots.

Theorem 2 (Behaviour of g_ε) *For $\varepsilon > 0$ g_ε has a unique maximum located at $0 < p^* < \infty$. For sufficiently small $\varepsilon > 0$ the maximum value is positive, i.e. $g_\varepsilon(p^*) > 0$, and g_ε has two roots p^- and p^+ such that $p^- < p^* < p^+$.*

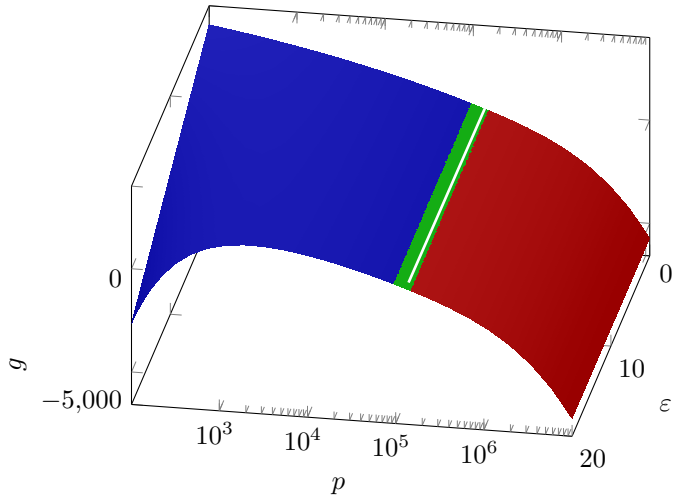

Fig. 3 Behaviour of g_ε for varying ε and p for $\overline{\boldsymbol{u}}_L = (1, 30, 1.5 \cdot 10^5)^T$ and $\boldsymbol{u}_R = (1, 30, 1.2 \cdot 10^5)^T$. Colour blue indicates the area where p corresponds to a two rarefaction wave solution, red to a two shock solution and green to a rarefaction and shock or vice versa. The white line on the surface marks the position of p^+.

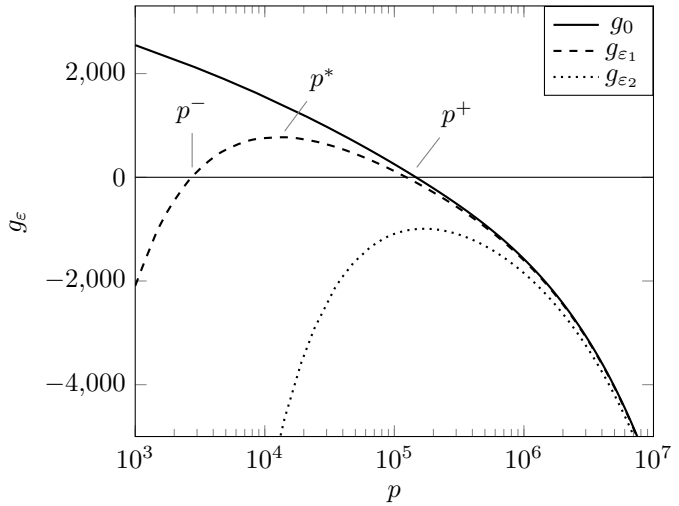

Fig. 4 Behaviour of g_ε for the classical RP and $\varepsilon_1 = 100$, $\varepsilon_2 = 1000$. For g_{ε_1} the left root p^-, the maximum p^* and the right root p^+ are annotated.

Proof Table 1 in the Appendix A entails the limits of g_ε towards the boundaries $p \to 0^+$ and $p \to \infty$. Since the limits of $(g_\varepsilon^1)'$ and $(g_\varepsilon^2)'$ coincide:

$$\lim_{p\to 0^+} (g^{1,2})'(p) \overset{RW}{=} -\infty, \quad \lim_{p\to\infty} (g^{1,2})'(p) \overset{SW}{=} 0^-, \tag{23}$$

they do not provide any information about the limits of g_ε'. Therefore, we investigate the limit of the derivative separately. Let $0 \le p \le \min\{p_L, p_R\}$, then

$$\lim_{p\to 0} g_\varepsilon'(p) \overset{RW}{=} \underbrace{-p^{-\frac{\gamma+1}{\gamma}}}_{\to\infty} \underbrace{\left(\left(\frac{c_L}{\gamma p_L} p_L^{\frac{\gamma+1}{2\gamma}} + \frac{c_R}{\gamma p_R} p_R^{\frac{\gamma+1}{2\gamma}} \right) p^{\frac{\gamma+1}{2\gamma}} - \varepsilon \frac{\tau_L}{\gamma} \right)}_{\to -\varepsilon\tau_L/\gamma} > 0. \tag{24}$$

Now let $p \geq \max\{p_L, p_R\}$, then

$$\begin{aligned}\lim_{p\to\infty} g_\varepsilon'(p) &\overset{SW}{=} -\frac{1}{\sqrt{2\rho_L}}\underbrace{\frac{(\gamma+1)p+(3\gamma-1)p_L}{(\gamma+1)p+(\gamma-1)p_L}}_{\to 1} - \frac{1}{\sqrt{2\rho_R}}\underbrace{\frac{(\gamma+1)p+(3\gamma-1)p_R}{(\gamma+1)p+(\gamma-1)p_R}}_{\to 1} \\ &+ \underbrace{\varepsilon\frac{4c_L^2}{\left((\gamma+1)p+(\gamma-1)p_R\right)^2}}_{\to 0} \\ &< 0.\end{aligned} \tag{25}$$

Since $g_\varepsilon \in C^2(\mathbb{R}^+)$ (see Appendix A.3) the mean value theorem implies that $g_\varepsilon'(p)$ has at least one root in $\mathbb{R}^+$. Thus, g_ε has at least one local maximum because of (24) and (25). The uniqueness of the maximum is obtained by examining the monotonicity of $(g_\varepsilon^1)'$ and $(g_\varepsilon^2)'$ respectively. As stated in equations (59), (60), (72) and (76) in Appendix A we have

$$(v_1^+)'' > 0, \qquad (v_1^+)''' < 0, \tag{26}$$

$$(v_3^-)'' < 0, \qquad (v_3^-)''' > 0 \tag{27}$$

on $\mathbb{R}_0^+$. Thus, for $(g_\varepsilon^1)' = (v_1^+)' - (v_3^-)'$ we conclude

$$(g_\varepsilon^1)'' > 0, \qquad (g_\varepsilon^1)''' < 0, \tag{28}$$

i.e. $(g_\varepsilon^1)'$ is strictly monotone increasing and concave. This also holds true for $(g_\varepsilon^2)' = \varepsilon(\tau_1^+)'$ since by equations (56), (57), (69) and (70):

$$(\tau_1^+)'' > 0, \qquad (\tau_1^+)''' < 0. \tag{29}$$

Consequently, $(g_\varepsilon^1)'$ and $(g_\varepsilon^2)'$ can have at most one intersection, otherwise $g_\varepsilon^{1,2}$ would exhibit inflection points, contradicting the monotonicity of $(g_\varepsilon^{1,2})'$. Thus, g_ε' has a single root in $\mathbb{R}^+$. Let p^* denote the location of the unique maximum.

Theorem 1 implies the existence of $\varepsilon_{\max} > 0$ such that for all $\varepsilon \in [0, \varepsilon_{max})$ a root p^+ of g_ε exists. Since g_ε has a unique maximum and $g_\varepsilon(p) \xrightarrow{p\to\infty} -\infty$ we have that $p^* < p^+$. Furthermore, a second root of g_ε at p^- with $p^- < p^*$ has to exist by reason of $g_\varepsilon(p) \xrightarrow{p\to 0} -\infty$. Finally, since p^* is the unique maximum and $p^- < p^* < p^+$ it must hold that $g_\varepsilon(p^*) > 0$.

□

For ε sufficiently small the location of p^* of the unique maximum can be determined explicitly.

Theorem 3 *In case ε is sufficiently small such that the states $\overline{\boldsymbol{u}}$ and $\boldsymbol{u}$ solving the coupling problem (10) are both located on the rarefaction branch of the Lax curves, the maximum value of g_ε and its location is known in closed form. Let*

$$A := \left(c_L p_L^{\frac{1-\gamma}{2\gamma}} + c_R p_R^{\frac{1-\gamma}{2\gamma}}\right), \quad B := \frac{\tau_L p_L^{\frac{1}{\gamma}}}{A} \text{ and } \quad C := \frac{2}{\gamma-1}A, \tag{30}$$

then

$$p^*(\varepsilon) = (\varepsilon B)^{\frac{2\gamma}{\gamma+1}} \tag{31}$$

and

$$g_\varepsilon(p^*(\varepsilon)) = g_\varepsilon(0) - \left(B^{\frac{\gamma-1}{\gamma+1}}C + \tau_L p_L^{\frac{1}{\gamma}} B^{-\frac{2}{\gamma+1}}\right)\varepsilon^{\frac{\gamma-1}{\gamma+1}}. \tag{32}$$

Furthermore, we determine $\bar{\varepsilon}_{max} \in \mathbb{R}^+$ as the largest value for which holds $g_\varepsilon(p^*) > 0 \ \ \forall \varepsilon \in [0, \bar{\varepsilon}_{max})$,

$$\bar{\varepsilon}_{max}^{\frac{\gamma-1}{\gamma+1}} = g_\varepsilon(0)\left(\tau_L p_L^{\frac{1}{\gamma}}\right)^{\frac{1-\gamma}{\gamma+1}} \frac{\gamma-1}{\gamma+1} A^{-\frac{2}{\gamma+1}}. \tag{33}$$

Proof In Appendix A.1 the addends of g_ε', $(v_{1,3}^{\pm})'$ and $(\tau_1^+)'$, are defined by equations (58) and (55), respectively. Solving the equation $g_\varepsilon' = 0$ for the case of two rarefaction waves, i.e. $p < \min\{p_L, p_R\}$ by means of elementary algebra yields the assertions.

□

Remark 1 For increasing values of ε the maximum $p^*(\varepsilon)$ decreases and thus the roots $p^-(\varepsilon)$ and $p^+(\varepsilon)$ are approaching each other until they coincide at some $\varepsilon = \varepsilon_{max}$. Note that $\bar{\varepsilon}_{max}$ coincides with ε_{max} in Theorem 2 if $p^* < \min\{p_L, p_R\}$. For $\varepsilon > \varepsilon_{max}$ the maximum of g_ε is negative, i.e. $g_\varepsilon(p^*(\varepsilon)) < 0$ and thus there exists no root of g_ε and, equivalently, no solution to the coupling problem (1).

Remark 2 For $\varepsilon \in (0, \varepsilon_{max})$ the singularity of g_ε at $p = 0$ behaves as $g_\varepsilon^2 \sim \frac{\varepsilon}{p}$ since $g_\varepsilon^1(0) \in \mathbb{R}^+$ in absence of vacuum states, cf. Appendix A. Hence, for $\varepsilon \to 0$ the singularity becomes increasingly steep and p^-, the left root of g_ε, approaches 0. At the same time, p^+, the right root of g_ε remains in the neighbourhood of the solution to the classical RP, as shown in the proof of Theorem 1. Consequently, p^- cannot be the physically admissible solution to the coupling problem.

Figures 3 and 4 demonstrate this behaviour. In particular, p^+ varies slowly for growing ε and even for comparably large values of ε the root p^+ is in a neighbourhood of the solution to the classical RP.

Conclusion 1 *For ε small enough $g_\varepsilon = 0$ has two solutions $p^-(\varepsilon)$ and $p^+(\varepsilon)$ where $p^+(\varepsilon)$ is the unique physically admissible solution of the coupling problem* (1)*.*

Finally, to obtain p^+ iterative methods such as of Newton type can be applied because g_ε is smooth and its derivative is known explicitly. The initial value p_0 has to be chosen such that $p_0 > p^*$. In case of $p^* < \min\{p_L, p_R\}$, i.e. the case of two rarefaction waves, p^* is given in closed form (31), otherwise $g_\varepsilon' = 0$ can be solved efficiently, since g_ε' has a unique root.

3 Coupled Riemann problem for the *p*-System

Since for many applications temperature dynamics can be neglected, the p-system is used as a simplified model for gas dynamics in pipe networks. In the following we show that a similar result as Theorem 2 is obtained for the p-system. Clearly, the analysis strongly shortens due to the simplified wave structure of the solutions to the p-system. For an isentropic flow the compressible Euler equations (2) reduce to the p-system

$$\begin{aligned} &\frac{\partial \rho}{\partial t} + \frac{\partial \rho v}{\partial x} = 0, \\ &\frac{\partial \rho v}{\partial t} + \frac{\partial}{\partial x}\left(\rho v^2 + p(\rho)\right) = 0. \end{aligned} \tag{34}$$

For the closure of the system we choose the γ-law

$$p(\rho) = \alpha \rho^\gamma \tag{35}$$

with $\gamma \geq 1$ and $\alpha > 0$. For $\rho > 0$ the pressure satisfies $p'(\rho) > 0$ and $p''(\rho) \geq 0$. Thus, the speed of sound is given by $c(\rho) = \sqrt{p'(\rho)}$ and we also assume that the flow at the interface is subsonic. We denote $\boldsymbol{u} := (\rho, \rho v)^T$ and adopt the same notation for the Lax curves as in the previous section. In an isentropic flow the temperature is constant and the coupling conditions (1) reduce to

$$\begin{aligned} \overline{\rho v} &= \rho v + \varepsilon, \\ \overline{p} &= p. \end{aligned} \tag{36}$$

The p-system is hyperbolic and the coupling problem in the sense of Definition 1 can be approached by means of Lax curves. However, in contrast to the compressible Euler equations, the solution of the classical RP is obtained in conserved variables $(\rho, \rho v)^T$ [35]. Thus, the solution to the two half–RPs satisfying the coupling conditions (36) is constructed in the same manner

as for the compressible Euler equations in Chapter 2, except that the Lax curves parameterised by the density ρ yield a scalar equation straightforwardly [2,22,7,3]. The Lax curves $L_i^{\pm}(\rho;\boldsymbol{u}) = (\rho, \rho v_i^{\pm})^T$ and their derivatives are summarised in Appendix B.

The coupling conditions (36) transform to

$$\begin{aligned} \overline{\rho} v_1^+(\overline{\rho}, \overline{\boldsymbol{u}}_L) &= \rho v_2^-(\rho, \boldsymbol{u}_R) + \varepsilon, \\ \overline{p} &= p. \end{aligned} \tag{37}$$

Since the pressure p depends continuously and monotonously on the density ρ, $\overline{p} = p$ implies $\overline{\rho} = \rho$. Due to the assumption of a subsonic flow the density in the solution of the RP is continuous at the coupling interface. The Lax curves are parameterised by ρ and therefore coupling conditions (37) reduce to a scalar equation. In order to solve the coupling problem we define the function $h_\varepsilon(\rho)$ as

$$h_\varepsilon \colon \mathbb{R} \to \mathbb{R}, \quad \rho \mapsto (\rho v)_1^+(\rho) - (\rho v)_2^+(\rho) - \varepsilon \tag{38}$$

and solve the equation $h_\varepsilon(\rho) = 0$. The behaviour of h_ε is illustrated in Figure 5 and analysed in Theorem 4 following hereafter.

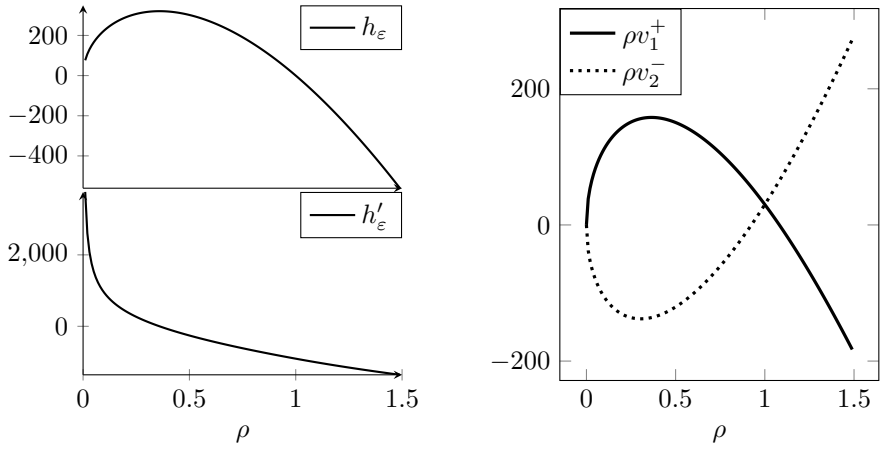

Fig. 5 Left from top to bottom: h_ε and its derivative h'_ε. The horizontal axes are aligned. Right: 1-wave and 2-wave for the momentum of the p-system in positive and negative direction respectively.

Theorem 4 *Let $\gamma \in (1,3)$ and $\varepsilon > 0$ sufficiently small. Then the coupling problem for the p-system has a unique solution.*

Proof As shown in Appendix B

$$h''_\varepsilon(\rho) < 0 \tag{39}$$

for non-negative ρ. That implies that $h'_\varepsilon(\rho)$ is strictly decreasing. Furthermore, for all $\varepsilon \geq 0$ and $\gamma \in (1,3)$

$$\lim_{\rho \to 0^+} h_\varepsilon(\rho) = -\varepsilon, \qquad \lim_{\rho \to \infty} h_\varepsilon(\rho) = -\infty, \tag{40}$$

$$\lim_{\rho \to 0^+} h'_\varepsilon(\rho) > 0, \qquad \lim_{\rho \to \infty} h'_\varepsilon(\rho) = -\infty. \tag{41}$$

Since h_ε is smooth, concave and has a positive derivative at $\rho = 0$ there must exist a global maximum whose position we denote by ρ^*. Thus, for ε small enough $h_\varepsilon(p^*) > 0$ and h_ε has two roots ρ^- and ρ^+ as well as a maximum at ρ^* such that $\rho^- < \rho^* < \rho^+$.

For $\varepsilon = 0$ the left root $\rho^- = 0$ corresponds to the vacuum state while the right root ρ^+ is the parameter that solves the classical RP. Applying the implicit function theorem as in the proof

of Theorem 1 yields an ε_{max} such that for $\varepsilon \in (0, \varepsilon_{max})$ ρ^+ is located in an open neighbourhood of the solution to the classical RP. In contrast to the compressible Euler equations the left root, viewed as a function of ε, $\rho^-(\varepsilon)$ approaches ρ^* *continuously* as $\varepsilon > 0$ increases. For $\varepsilon \in (0, \varepsilon_{max})$ ρ^- is located in an open neighbourhood of 0 and cannot be considered a physically admissible solution.

Hence, ρ^+ is the unique physically admissible solution of the coupling problem (36).

□

Remark 3 In an ideal gas the heat capacity ratio γ is linked with the degrees of freedom of a molecule f as

$$f = \frac{2}{\gamma - 1}, \tag{42}$$

see e.g. [37]. Since $f \in \mathbb{N}$ implies $\gamma \in (1, 3)$ the assumption on γ in Theorem 4 is not particularly restrictive.

Across rarefaction waves the density and the momentum of the solutions of the p-system and the compressible Euler equations are identical [35]. However, across shock waves the total energy may jump and the solutions can differ significantly. The p-system is suitable for many industrial applications such as natural gas pipeline networks where the gas is isothermal [30, 4]. However, if variations of the temperature become considerably high the p-system is not an adequate model and the full Euler equations yield the physically relevant description. This will also be illustrated in the numerical results.

4 Numerical results for the coupled Euler equations and the *p*-system

In order to solve the coupled problem we apply to both systems a Runge-Kutta discontinuous Galerkin method [6]. The performance is enhanced by local multi-resolution based grid adaptation, see [24, 14]. The solver is implemented in the Multiwave library [29]. The coupling procedure is carried out by computing the roots of g_ε and h_ε defined in (12) and (38), respectively, and setting the boundary conditions for the inflow and the outflow part. The details of the coupling procedure have been described in previous works, cf. [22].

We apply a third order DG scheme using polynomial elements of order $p = 3$ and a third-order SSP-Runge-Kutta method with three stages for the time-discretisation [17]. Both solvers use the same numerical flux, applied in the *interior* of each domain, and limiter, namely, the local Lax-Friedrichs flux and the minmod limiter from [6].

The start, operation and shutdown of a gas turbine are modelled by applying a time-dependent $\varepsilon = \varepsilon(t)$ to a steady flow where initially $\varepsilon(0) = 0$. We compute the solution of the coupling problem for three cases where each $\varepsilon(t)$ increases up to a constant value, maintains this constant value for a period of time and decreases back to zero.

The computational domain is $\Omega_S = [-200, 0]$ m for the inflow part and $\Omega_F = [0, 200]$ m for the outflow part. In each domain we use a base grid of 50 cells and $L = 8$ levels of refinement. Thus, the uniformly refined grid would consist of 50×2^8 cells that are never all used in the course of the computation. However, due to grid adaptation the locally refined grids consist of about 100 cells. The CFL number is set to 0.1 and the final time is $T = 0.55$ for the first case (Section 4.1) and $T = 0.09s$ for the second and the third case (Section 4.2).

The parameters of the equation of state (EoS) for the compressible Euler equations for the natural gas are given in [4] as

$$\gamma^{Euler} = 1.29, \quad R = 518.8. \tag{43}$$

In order to compare the solutions of the compressible Euler equations and of the p-system we set the pressure law for the p-system to

$$p(\rho) = 146820.4\rho, \tag{44}$$

i.e. $\gamma = 1$ for the p-system, since the EoS for the compressible Euler equations depends linearly on the density ρ.

4.1 The case of continuous outtake $\varepsilon(t)$

For the first case $\varepsilon = \varepsilon(t)$ is imposed to increase and decrease linearly and continuously,

$$\varepsilon(t) = \begin{cases} \min\{0.6, 3t\} & \text{if } 0 \le t < 0.3 \\ \max\{0, -3t + 0.6\} & \text{if } t \ge 0.3 \end{cases} . \tag{45}$$

We set the initial density $\rho(0,x) = 1kg/m^3$, the velocity $v(0,x) = 1m/s$. In addition for the compressible Euler equations the initial pressure is $p(0,t) = 146820.4Pa$. The resulting solution is presented in Figure 6.

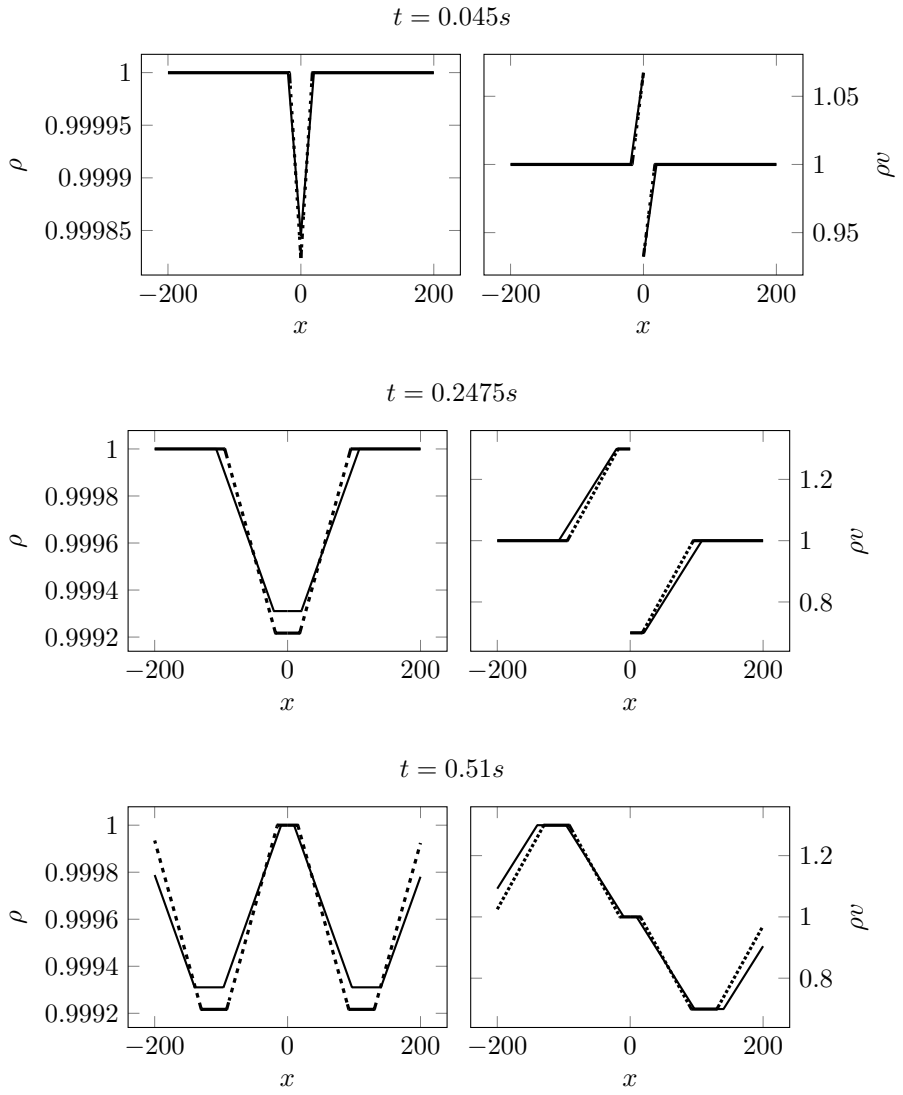

Fig. 6 Case 1. Continuously varying $\varepsilon(t)$. Dashed line - p-system, solid line - compressible Euler equations.

4.2 The case of discontinuous outtake $\varepsilon(t)$

In the second case we apply same initial conditions and EoS for the gas as in the first case, however, ε exhibits discontinuities,

$$\varepsilon(t) = \begin{cases} \tilde{\varepsilon} & \text{if } 0.01 \leq t < 0.05 \\ 0 & \text{otherwise} \end{cases}, \tag{46}$$

where $\tilde{\varepsilon} = 0.1$ is the magnitude of the jump, i.e. the momentum drained by the operating turbine. The results at final time are shown in Figure 7.

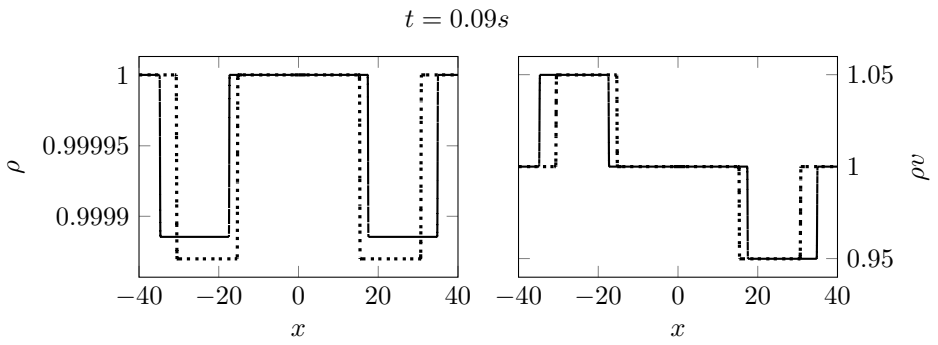

Fig. 7 Case 2. ε jumps from zero to 0.1 in a slower gas flow. Dashed line - p-system, solid line - compressible Euler equations.

For the third case we consider a faster gas flow in the pipe, i.e. we set $v(0, x) = 250m/s$ which corresponds to approximately $Ma = 0.56$. Furthermore, the jump in the momentum is $\tilde{\varepsilon} = 20.0$ while other data is as in the second case. Velocity that high is rarely found in a gas network, however, it allows to emphasise the differences between the p-system and the compressible Euler equations. Figure 8 presents the results for the faster flow at final time.

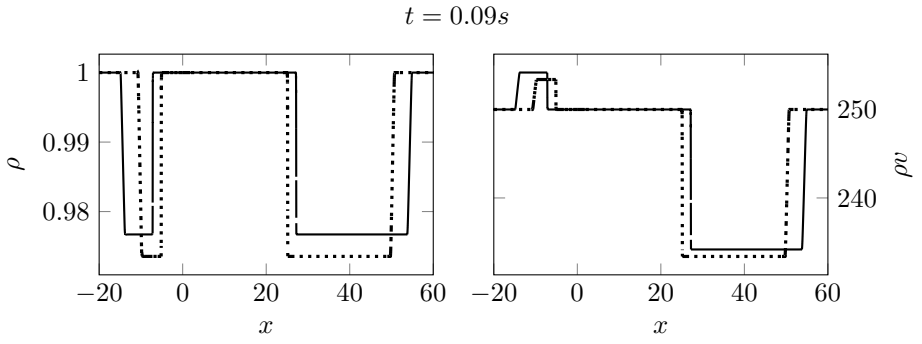

Fig. 8 Case 3. ε jumps from zero to 20.0 in a faster gas flow. Dashed line - p-system, solid line - compressible Euler equations.

4.3 Comparison and discussion of the numerical results

In the first and second case, where the flow velocity is comparably low, the differences between the compressible Euler equations and the p-system are moderate. In the solution of the compress-

ible Euler equations one can observe a variation of the temperature of a magnitude of $0.05K$. Furthermore, the waves in the solution of the p-systems are moving at a slightly higher speed since the gamma law does not account for the temperature. Hence, there is a difference in the pressure and therefore in the characteristic speeds.

In the third case, where the flow velocity is higher, the left and right moving leading waves emanating from the coupling interface are rarefactions. The magnitude of the rarefaction in the p-system solution is about 25% lower at the inflow and at the outflow as shown in Figure 9. The rarefaction waves are followed by shock waves corresponding to the turbine shutdown, i.e. ε jumping to zero. As mentioned in Section 3, the solution located on rarefaction waves is equal for the p-system and the compressible Euler equations. This can be seen in our simulations, albeit the magnitude and the different characteristic speeds.

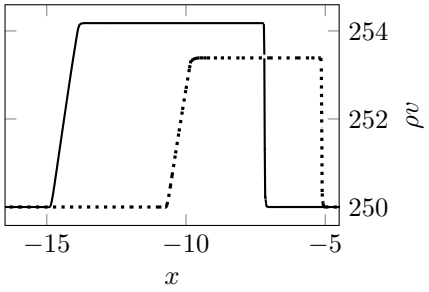

Fig. 9 Case 3. Zoom on the left-going waves at the inflow.

5 Conclusions

We have solved a coupling problem for the one-dimensional compressible Euler equations and the p-system, respectively. The coupling conditions impose a drop in the momentum at the coupling interface while other conserved quantities are continuous. This coupling problem has been solved by means of a generalised Riemann problem. The existence and uniqueness have been proven for constant initial data at the inflow and the outflow, respectively, and sufficiently small outtake of the momentum. Furthermore, the structure of the equation for the solution of the generalised Riemann problem has been analysed. In special cases the solution is given in a closed form and otherwise can be obtained efficiently by Newton type methods. Finally, theoretical results have been verified by numerical simulations of a gas turbine in the case of slow and fast moving gas. A comparison between the p-system and the Euler system has been conducted.

A Lax curves of the compressible Euler equations

The compressible Euler equations are a system of hyperbolic equations and therefore there exists an eigenvector decomposition of the flux Jacobian. For that reason, the self-similar solution of the classical RP can be constructed by means of Lax curves [35]. In this chapter we list the Lax curves for the simple waves in the subsonic case, i.e. the 1- and 3-wave, parameterised by the pressure p in primitive variables of the compressible Euler equations together with their first three derivatives with respect to p. Throughout we assume that the EoS is given by the ideal gas law (5).

The density along the Lax curves has the form

$$\rho_i^{\pm}(p) = \rho_0 - s_i^{\pm}\theta_i^{\pm}(p) \tag{47}$$

where i denotes the i-wave, $^{\pm}$ the direction on the Lax curve and $s_i^{\pm} := \pm(2-i) \in \{-1, 1\}, i \in \{1, 3\}$ is a sign term depending on these two parameters. The subscript $_0$ denotes the foot-point of the Lax curve. The term $\theta_i^{\pm}$ will be specified in the following sections where we distinguish between the rarefaction and the shock wave. The velocity Lax curves will also be specified in the next two sections, since its structure differs for the simple wave types.

A.1 Rarefaction wave

For the rarefaction wave the term $\theta_i^{\pm}$ reads

$$\theta_i^{\pm}(p) := -\rho_0 \left(\left(\frac{p}{p_0} \right)^{\frac{1}{\gamma}} - 1 \right) s_i^{\pm}. \tag{48}$$

Thus, by means of elementary algebra the density Lax curve for the rarefaction case can be written as a rational function of p:

$$\rho_i^{\pm}(p) = \rho_0 \left(\frac{p}{p_0} \right)^{1/\gamma}. \tag{49}$$

The velocity Lax curve is given by

$$v_i^{\pm}(p) = v_0 \pm \frac{2c_0}{\gamma - 1} r_i^{\pm}(p), \tag{50}$$

where

$$r_i^{\pm}(p) := s_i^{\pm} \left(1 - \left(\frac{p}{p_0} \right)^{\frac{\gamma-1}{2\gamma}} \right). \tag{51}$$

Since by definition of the compressible Euler equations $p, p_0, \rho_0 > 0$ and $\gamma > 1$, we have

$$\theta_i^{\pm} \geq 0 \Leftrightarrow s_i^{\pm} p_0 \geq s_i^{\pm} p \tag{52}$$

and

$$r_i^{\pm} \leq 0 \Leftrightarrow s_i^{\pm} p_0 \geq s_i^{\pm} p. \tag{53}$$

Recall that the specific volume at the foot-point of the Lax curves reads $\tau_0 = 1/\rho_0$, thus we have

$$\tau_i^{\pm}(p) := \frac{1}{\rho_i^{\pm}(p)} = \tau_0 \left(\frac{p_0}{p} \right)^{\frac{1}{\gamma}}. \tag{54}$$

The derivatives of τ have the following sign:

$$\frac{\mathrm{d}\tau_i^{\pm}}{\mathrm{d}p}(p) = -\frac{\tau_0}{\gamma} p_0^{\frac{1}{\gamma}} p^{-\left(1+\frac{1}{\gamma}\right)} < 0, \tag{55}$$

$$\frac{\mathrm{d}^2\tau_i^{\pm}}{\mathrm{d}p^2}(p) = (\gamma+1)\frac{\tau_0}{\gamma^2} p_0^{\frac{1}{\gamma}} p^{-\left(2+\frac{1}{\gamma}\right)} > 0, \tag{56}$$

$$\frac{\mathrm{d}^3\tau_i^{\pm}}{\mathrm{d}p^3}(p) = -(\gamma+1)\frac{\tau_0 p^{\frac{1}{\gamma}}}{\gamma^3}(2\gamma+1) p^{-\frac{3\gamma+1}{\gamma}} < 0, \tag{57}$$

while the derivatives of the velocity Lax curves read

$$\frac{\mathrm{d}v_i^{\pm}}{\mathrm{d}p}(p) = \mp s_i^{\pm} \frac{c_0}{\gamma p_0} \left(\frac{p}{p_0} \right)^{-\frac{\gamma+1}{2\gamma}}, \tag{58}$$

$$\frac{\mathrm{d}^2 v_i^{\pm}}{\mathrm{d}p^2}(p) = -\frac{\gamma+1}{2\gamma p} \frac{\mathrm{d}v_i^{\pm}}{\mathrm{d}p}(p), \tag{59}$$

$$\frac{\mathrm{d}^3 v_i^{\pm}}{\mathrm{d}p^3}(p) = \mp s_i^{\pm} \frac{c_0(\gamma+1)(3\gamma+1)}{4\gamma^3 p_0^3} \left(\frac{p}{p_0} \right)^{-\frac{5\gamma+1}{2\gamma}}, \tag{60}$$

where $\operatorname{sgn}\left(\frac{\mathrm{d}^3 v_i^{\pm}}{\mathrm{d}p^3} \right) = \mp s_i^{\pm}$.

A.2 Shock wave

This section resembles Section A.1 for the case of shock wave Lax curves. The density Lax curves read

$$\rho_i^{\pm}(p) = \rho_0 \frac{(\gamma+1)p + (\gamma-1)p_0}{(\gamma-1)p + (\gamma+1)p_0} \tag{61}$$

and the velocity Lax curve

$$v_i^{\pm}(p) = v_0 \pm \left(r_i^{\pm}(p) \right)^{-\frac{1}{2}} c_0 \theta_i^{\pm}(p) = v_0 \pm s_i^{\pm} \left(r_i^{\pm}(p) \right)^{-\frac{1}{2}} c_0 (\rho_0 - \rho_i^{\pm}(p)), \tag{62}$$

where

$$\theta_i^{\pm}(p) := s^{\pm}\frac{2\rho_0(p_0-p)}{(\gamma-1)p+(\gamma+1)p_0} = s_i^{\pm}(\rho_0-\rho_i^{\pm}(p)) \tag{63}$$

and

$$r_i^{\pm}(p) := \frac{1}{2}\left(2\rho_0 + s_i^{\pm}(\gamma-1)\theta_i^{\pm}(p)\right)\rho_i^{\pm}(p). \tag{64}$$

By definition of the compressible Euler equation $p, p_0, \rho_0 > 0$ and $\gamma > 1$ holds and thus we obtain

$$\theta_i^{\pm} \le 0 \Leftrightarrow s_i^{\pm}(p_0-p) \le 0 \tag{65}$$

and

$$r_i^{\pm} \ge 0 \Leftrightarrow c_0^2 \ge 0. \tag{66}$$

The specific volume Lax curve reads

$$\tau_i^{\pm}(p) := \frac{1}{\rho_i^{\pm}(p)} = \tau_0\frac{(\gamma-1)p+(\gamma+1)p_0}{(\gamma+1)p+(\gamma-1)p_0} \tag{67}$$

and its derivatives are

$$\frac{\mathrm{d}\tau_i^{\pm}}{\mathrm{d}p}(p) = -\frac{4c_0^2}{\left((\gamma+1)p+(\gamma-1)p_0\right)^2} < 0, \tag{68}$$

$$\frac{\mathrm{d}^2\tau_i^{\pm}}{\mathrm{d}p^2}(p) = \frac{8c_0^2(\gamma+1)}{\left((\gamma+1)p+(\gamma-1)p_0\right)^3} > 0, \tag{69}$$

$$\frac{\mathrm{d}^3\tau_i^{\pm}}{\mathrm{d}p^3}(p) = \frac{-24c_0^2(\gamma+1)^2}{\left((\gamma+1)p+(\gamma-1)p_0\right)^4} < 0. \tag{70}$$

The derivatives of the velocity Lax curves are slightly complicated for the shock wave case and we examine them separately. The first derivative of the velocity Lax curve reads

$$\frac{\mathrm{d}v_i^{\pm}}{\mathrm{d}p}(p) = \mp s_i^{\pm}\frac{1}{\sqrt{2}}\rho_0^{-\frac{1}{2}}\frac{(\gamma+1)p+(3\gamma-1)p_0}{\left((\gamma+1)p+(\gamma-1)p_0\right)^{\frac{3}{2}}}, \tag{71}$$

and the second derivative is

$$\frac{\mathrm{d}^2v_i^{\pm}}{\mathrm{d}p^2}(p) = \pm s_i^{\pm}c_0\frac{1}{\gamma-1}\frac{1}{\sqrt{8\gamma p_0}}\frac{\left((\gamma+1)p+(\gamma-1)p_0\right)^{-\frac{5}{2}}}{(\gamma-1)p+(\gamma+1)p_0}q(p), \tag{72}$$

where $q(p)$ is polynomial in p defined as

$$q(p) := (\gamma^2-1)^2p^2 + 2(\gamma^2-1)q_1(\gamma)pp_0 + (\gamma^2+1)^2q_2(\gamma)p_0^2 \tag{73}$$

with

$$q_1(\gamma) := 4\gamma^2 - 3\gamma + 1 > 0, \tag{74}$$

$$q_2(\gamma) := 7\gamma^2 - 8\gamma + 1 = (\gamma-1)(7\gamma-1) > 0 \tag{75}$$

for $\gamma > 1$. Finally, we state the third derivative of the velocity Lax curve:

$$\frac{\mathrm{d}^3v_i^{\pm}}{\mathrm{d}p^3}(p) = \mp s_i^{\pm}\frac{c_0(\gamma+1)}{4\sqrt{2\gamma p_0}}\frac{\left((\gamma+1)p+(\gamma-1)p_0\right)^{-\frac{7}{2}}}{\left((\gamma-1)p+(\gamma+1)p_0\right)^2}\left(q_1'p^3 + q_2'p^2p_0 + q_3'pp_0^2 + q_4'p_0^3\right), \tag{76}$$

where the coefficients $q_i' \in \mathbb{R}$ read

$$q_1' = 3(\gamma^2-1)^2 > 0, \tag{77}$$

$$q_2' = (39\gamma^2 - 24\gamma + 9)(\gamma^2-1) > 0, \tag{78}$$

$$q_3' = (69\gamma^2 - 66\gamma + 9)(\gamma+1)^2 > 0, \tag{79}$$

$$q_4' = (33\gamma^2 + 30\gamma - 3)(\gamma+1)^2 > 0. \tag{80}$$

The inequalities hold for $\gamma > 1$.

A.3 Properties of the Lax curves derivatives and convexity of g_ε

The functions $\tau_i^\pm$ and $v_i^\pm$ belong both to $C^2(\mathbb{R}^+\backslash\{0\})$ but the third derivatives have a jump in p_0 and thus are *are not continuous:*

$$\lim_{p\to p_0^-} \frac{\mathrm{d}^3 v_i^\pm}{\mathrm{d}p^3} = \mp s_i^\pm \frac{c_0(\gamma+1)}{(3\gamma+1)} 4\gamma^3 p_0^3 \neq \mp s_i^\pm \frac{c_0(\gamma+1)^2}{\gamma^3 p_0^3} = \lim_{p\to p_0^+} \frac{\mathrm{d}^3 v_i^\pm}{\mathrm{d}p^3}, \tag{81}$$

$$\lim_{p\to p_0^-} \frac{\mathrm{d}^3 \tau_i^\pm}{\mathrm{d}p^3} = -\frac{(\gamma+1)(2\gamma+1)}{\gamma^3}\frac{\tau_0}{p_0^3} \neq -\frac{3}{2}\frac{(\gamma+1)^2}{(\gamma p_0)^3}\tau_0 = \lim_{p\to p_0^+} \frac{\mathrm{d}^3 \tau_i^\pm}{\mathrm{d}p^3}. \tag{82}$$

Furthermore, we can conclude from the previous discussion of the Lax curves for the compressible Euler equations the following Lemma.

Lemma 1 $\mathrm{sgn}(g_\varepsilon'')$ *is varying, however* g_ε *is concave for* $p \ll 1$ *and convex for* $p \gg 1$.

Proof By equations (59) and (72) v_1^+ is convex and v_3^- is concave, hence g_ε^1 is convex. Furthermore, by (56) and (69), g_ε^2 is also convex, i.e.

$$g_\varepsilon(p) = \underbrace{g_\varepsilon^1(p)}_{convex} - \underbrace{g_\varepsilon^2(p)}_{convex}. \tag{83}$$

Note that g_ε^1 dominates the behaviour of g_ε for $p \to 0$ and g_ε^2 for $p \to \infty$.

A.4 Limits of the Euler equations Lax curves and its derivatives

We state the limits of the Lax curves for the compressible Euler equations towards 0 and ∞ in Table 1.

	Rarefaction		Shock	
f	$\lim_{p\to 0} f$	$\lim_{p\to\infty} f$	$\lim_{p\to 0} f$	$\lim_{p\to\infty} f$
$\tau_i^\pm$	∞	0	$\tau_0 \frac{\gamma+1}{\gamma-1}$	$\tau_0 \frac{\gamma-1}{\gamma+1}$
$v_i^\pm$	$v_0 \pm \frac{2c_0}{\gamma-1} s_i^\pm$	$\mathrm{sgn}(\mp s_i^\pm)\cdot\infty$	$v_0 \pm \frac{2c_0}{\gamma-1} s_i^\pm$	$\mathrm{sgn}(\mp s_i^\pm)\cdot\infty$
$(\tau_i^\pm)'$	$-\infty$	0^-	$-\frac{4\gamma}{(\gamma-1)^2}\frac{\tau_0}{p_0}$	0^-
$(v_i^\pm)'$	$\mathrm{sgn}(\mp s_i^\pm)\cdot\infty$	$0\cdot\mathrm{sgn}(\mp s_i^\pm)$	$\mp s_i^\pm \frac{1}{\sqrt{2\gamma}}\frac{c_0}{p_0}\frac{3\gamma-1}{(\gamma-1)^{3/2}}$	$0\cdot\mathrm{sgn}(\pm s_i^\pm)$
$(\tau_i^\pm)''$	∞	0^+	$\frac{8c_0^2(\gamma+1)}{((\gamma-1)p_0)^3}$	0^+
$(v_i^\pm)''$	$\mathrm{sgn}(\pm s_i^\pm)\cdot\infty$	$0\cdot\mathrm{sgn}(\pm s_i^\pm)$	$\pm s_i^\pm \frac{c_0}{\sqrt{8\gamma}}\frac{(\gamma+1)}{(\gamma-1)^{5/2}}\frac{7\gamma-1}{p_0^2}$	$0\cdot\mathrm{sgn}(\pm s_i^\pm)$
$(\tau_i^\pm)'''$	$-\infty$	0^-	$-\frac{24c_0^2(\gamma+1)^2}{((\gamma-1)p_0)^4}$	0^-
$(v_i^\pm)'''$	$\mathrm{sgn}(\mp s_i^\pm)\cdot\infty$	$0\cdot\mathrm{sgn}(\mp s_i^\pm)$	$\pm s_i^\pm \frac{c_0}{4\sqrt{2\gamma}}\frac{(\gamma-1)^{-9/2}}{(\gamma+1)^2 p_0^3} q_4$	$0\cdot\mathrm{sgn}(\pm s_i^\pm)$

Table 1 Compressible Euler equations: Limits of the Lax curves, $\tau_i^\pm$ and $v_i^\pm$, and their derivatives for the rarefaction wave and the shock wave branches.
Notation: By $\lim f = 0^\pm$ we emphasise that f approaches 0 either from the positive or from the negative direction.

B Lax curves of the *p*-system

In this section we summarize the Lax curves and their derivatives and limits for the p-system which is, like the full Euler equations, a hyperbolic system. Furthermore, we prove that h_ε is convex, an important property employed in the proof of Theorem 4. The analysis performed in Appendix A simplifies a lot since the Lax curves are parameterised by ρ and the solution of the coupling problem is found by solving the equation $h_\varepsilon(\rho) = 0$ which depends only on the momentum Lax curves.

First, we state the 1-wave and 2-wave momentum Lax curves for the rarefaction and shock case [7]. We adopt the notation of Appendix A. Recall that the pressure is governed by the γ-law, i.e. $p(\rho) = \alpha\rho^\gamma$ with $\alpha > 0$ and $\gamma \geq 1$. Then the 1-forward Lax curve and the 2-backward Lax-curve are

$$L_1^+(\rho, \boldsymbol{u}_0) = \begin{cases} R_1(\rho; \boldsymbol{u}_0) & \text{if } \rho < \rho_0 \\ S_1(\rho; \boldsymbol{u}_0) & \text{if } \rho > \rho_0 \end{cases}, \tag{84}$$

$$L_2^-(\rho, \boldsymbol{u}_0) = \begin{cases} S_2(\rho; \boldsymbol{u}_0) & \text{if } \rho > \rho_0 \\ R_2(\rho; \boldsymbol{u}_0) & \text{if } \rho < \rho_0 \end{cases}, \tag{85}$$

where R_i and S_i denote the rarefaction and the shock wave, respectively. The **rarefaction branches** of the Lax curves are given by

$$R_i = \rho v_0 - s_i \rho \int_{\rho_0}^{\rho} \frac{c(r)}{r} dr = \begin{cases} \rho v_0 - s_i \rho \sqrt{\alpha} (\ln \rho - \ln \rho_0) & \text{if } \gamma = 1 \\ \rho v_0 - s_i \sqrt{\alpha\gamma} \frac{2}{\gamma - 1} \left(\rho^{\frac{\gamma+1}{2}} - \rho_0^{\frac{\gamma-1}{2}} \rho \right) & \text{if } \gamma > 1 \end{cases}, \tag{86}$$

where

$$s_i := \begin{cases} 1 & \text{if } i = 1 \\ -1 & \text{if } i = 2 \end{cases}$$

is a sign term depending on the i-wave. The **shock branches** of the Lax curves read:

$$S_i(\rho; \boldsymbol{u}_0) = \rho v_0 - s_i \sqrt{s(\rho; \boldsymbol{u}_0)}, \tag{87}$$

where the discriminant is defined as $s(\rho; \boldsymbol{u}_0) := \frac{\rho}{\rho_0}(\rho - \rho_0)(p(\rho) - p(\rho_0))$.

Lemma 2 *The γ-law for the pressure has the following properties:*

$$p'(\rho) = \alpha\gamma\rho^{\gamma-1} = \gamma p(\rho)/\rho > 0, \tag{88}$$

$$p''(\rho) = \gamma(\gamma - 1)p(\rho)/\rho^2 \geq 0, \tag{89}$$

$$p'''(\rho) = \gamma(\gamma - 1)(\gamma - 2)p(\rho)/\rho^3. \tag{90}$$

Proof The derivatives are obtained using elementary calculus. □

Next, we compute the derivatives of the momentum Lax curves. For the **rarefaction branches** we obtain:

$$\frac{\mathrm{d}R_i}{\mathrm{d}p}(p) = v_0 + s_i \int_{\rho}^{\rho_0} \frac{c(r)}{r} dr - s_i c(\rho), \tag{91}$$

$$\frac{\mathrm{d}^2 R_i}{\mathrm{d}p^2}(p) = -s_i \frac{c(\rho)}{\rho} + s_i c'(\rho) = -s_i \underbrace{\frac{2c^2(\rho) + \rho p''(\rho)}{2\rho c(\rho)}}_{>0}, \tag{92}$$

where the inequality holds by Lemma 2. For the **shock branches** we have the following derivatives:

$$\frac{\mathrm{d}S_i}{\mathrm{d}p}(p) = v_0 - s_i \frac{s'(\rho)}{2\sqrt{s(\rho)}}, \tag{93}$$

$$\frac{\mathrm{d}^2 S_i}{\mathrm{d}p^2}(p) = -s_i \frac{1}{2\sqrt{s(\rho)}} \left(s''(\rho) - \frac{(s'(\rho))^2}{2s(\rho)} \right). \tag{94}$$

$$\tag{95}$$

We assume that $s'''(\rho) > 0$ holds. Then it was proven in [19] that for $\rho \leq \rho_0$ the rarefaction branches R_1 and R_2 are concave and convex, respectively, whereas for $\rho > \rho_0$ the shock branches S_1 and S_2 are concave and convex, respectively. We conclude that the function

$$h_\varepsilon(\rho) = \underbrace{L_1^+(\rho; \boldsymbol{u}_0)}_{\text{concave}} - \underbrace{L_2^-(\rho; \boldsymbol{u}_0)}_{\text{convex}} - \varepsilon$$

defined for the sake of finding the solution to the coupling problem for the p-system is concave, i.e. $h_\varepsilon''(\rho) < 0$.

Finally, we calculate the limits of the momentum Lax curves and their derivatives for $\rho \to 0$ and $\rho \to \infty$. For $\rho \to 0$ the state on the Lax curve corresponds to the rarefaction branch:

$$\lim_{\rho \to 0+} R_{1,2}(\rho; \boldsymbol{u}_0) = 0, \tag{96}$$

whereas for $\rho \to \infty$ to the shock branch:

$$\lim_{\rho \to +\infty} S_{1,2}(\rho; \boldsymbol{u}_0) = -s_i \cdot \infty. \tag{97}$$

Thus, $\lim_{\rho \to 0} h_\varepsilon = -\varepsilon$ and $\lim_{\rho \to 0} h_\varepsilon = -\infty$.

Next, we calculate the limit of the derivative of h_ε. For $\rho \leq \min\{\bar{\rho}_L, \rho_R\}$

$$\lim_{\rho \to 0+} h'_\varepsilon(\rho) = \bar{v}_L - v_R + \begin{cases} 2c \cdot \infty, & \gamma = 1 \\ \frac{2}{\gamma - 1}(c(\bar{\rho}_L) + c(\rho_R)) & \gamma > 1 \end{cases} = \begin{cases} \infty, & \gamma = 1 \\ \bar{v}_L - v_R + \frac{2}{\gamma - 1}(\bar{c}_L + c_R) & \gamma > 1 \end{cases}. \tag{98}$$

For subsonic states and $\gamma > 1$ it follows

$$\lim_{\rho \to 0+} h'_\varepsilon(\rho) = \bar{v}_L - v_R + \frac{2}{\gamma - 1}(\bar{c}_L + c_R) \tag{99}$$

$$\leq \bar{c}_L + c_R + \frac{2}{\gamma - 1}(\bar{c}_L + c_R) \tag{100}$$

$$= \frac{\gamma + 1}{\gamma - 1}(\bar{c}_L + c_R) \tag{101}$$

and

$$\lim_{\rho \to 0+} h'_\varepsilon(\rho) = \bar{v}_L - v_R + \frac{2}{\gamma - 1}(\bar{c}_L + c_R) \tag{102}$$

$$\geq -\bar{c}_L - c_R + \frac{2}{\gamma - 1}(\bar{c}_L + c_R) \tag{103}$$

$$= \frac{3 - \gamma}{\gamma - 1}(\bar{c}_L + c_R) \tag{104}$$

Hence,

$$\frac{3 - \gamma}{\gamma - 1}(\bar{c}_L + c_R) \leq \lim_{\rho \to 0+} h'_\varepsilon(\rho) \leq \frac{\gamma + 1}{\gamma - 1}(\bar{c}_L + c_R) \tag{105}$$

and for $\gamma \in (1, 3)$ we conclude

$$\lim_{\rho \to 0+} h'_\varepsilon(\rho) > 0. \tag{106}$$

In a similar manner, after cumbersome calculations we obtain

$$\lim_{\rho \to \infty} h_\varepsilon = \infty.$$

References

1. An, S., Li, Q., Gedra, T.W.: Natural gas and electricity optimal power flow. In: 2003 IEEE PES Transmission and Distribution Conference and Exposition (IEEE Cat. No.03CH37495), vol. 1, pp. 138–143 (2003). DOI 10.1109/TDC.2003.1335171
2. Banda, M.K., Herty, M., Klar, A.: Gas flow in pipeline networks. Netw. Heterog. Media **1**(1), 41–56 (2006). DOI 10.3934/nhm.2006.1.41. URL http://dx.doi.org/10.3934/nhm.2006.1.41
3. Bressan, A., Canic, S., Garavello, M., Herty, M., Piccoli, B.: Flow on networks: recent results and perspectives. European Mathematical Society-Surveys in Mathematical Sciences **1**(1), 47–111 (2014)
4. Brouwer, J., Gasser, I., Herty, M.: Gas pipeline models revisited: model hierarchies, nonisothermal models, and simulations of networks. Multiscale Model. Simul. **9**(2), 601–623 (2011). DOI 10.1137/100813580. URL http://dx.doi.org/10.1137/100813580
5. Chertkov, M., Fisher, M.W., Backhaus, S., Bent, R., Misra, S.: Pressure fluctuations in natural gas networks caused by gas-electric coupling. 2015 48th Hawaii Int. Conf. Syst. Sci. pp. 2738–2747 (2015)
6. Cockburn, B., Shu, C.W.: The Runge–Kutta discontinuous Galerkin method for conservation laws V: Multidimensional systems. J. Comput. Phys. **141**(2), 199–224 (1998). DOI https://doi.org/10.1006/jcph.1998.5892
7. Colombo, R.M., Garavello, M.: On the Cauchy problem for the p-system at a junction. SIAM J. Math. Anal. **39**(5), 1456–1471 (2008). DOI 10.1137/060665841
8. Colombo, R.M., Herty, M., Sachers, V.: On 2×2 conservation laws at a junction. SIAM J. Math. Anal. **40**(2), 605–622 (2008)

9. Colombo, R.M., Mauri, C.: Euler system at a junction. Journal of Hyperbolic Differential Equations **5**(3), 547–568 (2007)
10. Dafermos, C.M.: Hyperbolic Conservation Laws in Continuum Physics, 4th edn. Grundlehren der mathematischen Wissenschaften. Springer-Verlag (2016)
11. Dubois, F., Le Floch, P.: Boundary conditions for nonlinear hyperbolic systems of conservation laws. Journal of Differential Equations **71**(1), 93–122 (1988). DOI 10.1016/0022-0396(88)90040-X
12. Ehrhardt, K., Steinbach, M.C.: KKT systems in operative planning for gas distribution networks. PAMM **4**(1), 606–607 (2004)
13. Evans, P.C., Farina, M.F.: The age of gas & the power of networks. https://www.ge.com/sites/default/files/GE_Age_of_Gas_Whitepaper_20131014v2.pdf, GE (2013)
14. Gerhard, N., Iacono, F., May, G., Müller, S., Schäfer, R.: A high-order discontinuous Galerkin discretization with multiwavelet-based grid adaptation for compressible flows. J. Sci. Comput. **62**(1), 25–52 (2015). DOI 10.1007/s10915-014-9846-9
15. Godlewski, E., Le Thanh, K.C., Raviart, P.A.: The numerical interface coupling of nonlinear hyperbolic systems of conservation laws: II. The case of systems. ESAIM: Mathematical Modelling and Numerical Analysis **39**(4), 649–692 (2010)
16. Godlewski, E., Raviart, P.A.: Numerical Approximation of Hyperbolic Systems of Conservation Laws. Applied Mathematical Sciences. Springer-Verlag (1996)
17. Gottlieb, S., Shu, C.W., Tadmor, E.: Strong stability-preserving high-order time discretization methods. SIAM Rev. **43**, 89–112 (2001)
18. Grundel, S., Hornung, N., Roggendorf, S.: Numerical aspects of model order reduction for gas transportation networks. In: S. Koziel, L. Leifsson, X.S. Yang (eds.) Simulation-Driven Modeling and Optimization, Springer Proceedings in Mathematics & Statistics, pp. 1–28. Springer International Publishing (2016)
19. Gugat, M., Herty, M., Müller, S.: Coupling conditions for the transition from supersonic to subsonic fluid states. Netw. Heterog. Media **12**, 371–380 (2017). DOI 10.3934/nhm.2017016
20. Herty, M.: Modeling, simulation and optimization of gas networks with compressors. Netw. Heterog. Media **2**(1), 81–97 (2007). DOI 10.3934/nhm.2007.2.81. URL http://dx.doi.org/10.3934/nhm.2007.2.81
21. Herty, M., Mohring, J., Sachers, V.: A new model for gas flow in pipe networks. Math. Methods Appl. Sci. **33**(7), 845–855 (2010). DOI 10.1002/mma.1197. URL http://dx.doi.org/10.1002/mma.1197
22. Herty, M., Müller, S., Gerhard, N., Xiang, G., Wang, B.: Fluid-structure coupling of linear elastic model with compressible flow models: Coupling of linear elastic model with compressible flow models. Int. J. Numer. Methods Fluids **86**(6), 365–391 (2018). DOI 10.1002/fld.4422
23. Herty, M., Sachers, V.: Adjoint calculus for optimization of gas networks. Netw. Heterog. Media **2**(4), 733–750 (2007). DOI 10.3934/nhm.2007.2.733. URL http://dx.doi.org/10.3934/nhm.2007.2.733
24. Hovhannisyan, N., Müller, S., Schäfer, R.: Adaptive multiresolution discontinuous Galerkin schemes for conservation laws. Math. Comput. **83**, 113–151 (2014). DOI 10.1090/S0025-5718-2013-02732-9
25. Ibrahim, T.K., Basrawi, F., Awad, O.I., Abdullah, A.N., Najafi, G., Mamat, R., Hagos, F.Y.: Thermal performance of gas turbine power plant based on exergy analysis. Applied Thermal Engineering **115**, 977–985 (2017). DOI 10.1016/j.applthermaleng.2017.01.032
26. Kolb, O., Lang, J., Bales, P.: An implicit box scheme for subsonic compressible flow with dissipative source term. Numer. Algorithms **53**(2-3), 293–307 (2010). DOI 10.1007/s11075-009-9287-y. URL http://dx.doi.org/10.1007/s11075-009-9287-y
27. Ma, F., Jiao, Z., Li, Z., Wang, Y.: Impacts of gas network emergencies on power system through gas turbine. In: 2017 IEEE International Conference on Environment and Electrical Engineering and 2017 IEEE Industrial and Commercial Power Systems Europe (EEEIC / I CPS Europe), pp. 1–5 (2017). DOI 10.1109/EEEIC.2017.7977809
28. Martin, A., Moeller, M., Moritz, S.: Mixed integer models for the stationary case of gas network optimization. Math. Program. **105**, 563–582 (2005)
29. Müller, S., Sikstel, A.: Multiwave. https://www.igpm.rwth-aachen.de/forschung/multiwave, Institut für Geomtrie und Praktische Mathematik, RWTH Aachen (2018)
30. Osiadacz, A.: Simulation of transient flow in gas networks. Int. Journal for Numerical Methods in Fluid Dynamics **4**, 13–23 (1984)
31. Ríos-Mercado, R.Z., Borraz-Sánchez, C.: Optimization problems in natural gas transportation systems: A state-of-the-art review. Applied Energy **147**, 536–555 (2015). DOI 10.1016/j.apenergy.2015.03.017
32. Rowen, W.I.: Simplified mathematical representations of single shaft gas turbines in mechanical drive service. In: ASME 1992 International Gas Turbine and Aeroengine Congress and Exposition, vol. 5 (1992). DOI 10.1115/92-GT-022
33. Schmidt, M., Steinbach, M.C., Willert, B.M.: High detail stationary optimization models for gas networks. Optim. Eng. **16**(1), 131–164 (2015). DOI 10.1007/s11081-014-9246-x. URL http://dx.doi.org/10.1007/s11081-014-9246-x
34. Steinbach, M.C.: On PDE solution in transient optimization of gas networks. J. Comput. Appl. Math. **203**(2), 345–361 (2007). DOI 10.1016/j.cam.2006.04.018. URL http://dx.doi.org/10.1016/j.cam.2006.04.018
35. Toro, E.F.: Riemann Solvers and Numerical Methods for Fluid Dynamics: A Practical Introduction, 3 edn. Springer (2009)
36. Unsihuay, C., Lima, J.W.M., de Souza, A.C.Z.: Modeling the integrated natural gas and electricity optimal power flow. In: 2007 IEEE Power Engineering Society General Meeting, pp. 1–7 (2007). DOI 10.1109/PES.2007.386124
37. Wedler, G.: Lehrbuch der physikalischen Chemie. Wiley (2005)

38. Zhou, J., Adewumi, M.A.: Simulation of transients in natural gas pipelines using hybrid TVD schemes. Int. J. Numer. Meth. Fluids **32**, 407–437 (2000)
39. Zlotnik, A., Chertkov, M., Backhaus, S.: Optimal control of transient flow in natural gas networks. In: Decision and Control (CDC), 2015 IEEE 54th Annual Conference on, pp. 4563–4570. IEEE (2015)
40. Zlotnik, A., Roald, L., Backhaus, S., Chertkov, M., Andersson, G.: Control policies for operational coordination of electric power and natural gas transmission systems. In: 2016 American Control Conference (ACC), pp. 7478–7483 (2016). DOI 10.1109/ACC.2016.7526854